Applied Catalysis B: Environmental 224 (2018) 508–517

Contents lists available at ScienceDirect

Applied Catalysis B: Environmental

journal homepage: www.elsevier.com/locate/apcatb

Research paper

Carbon dots-TiO_2 nanosheets composites for photoreduction of Cr(VI) under sunlight illumination: Favorable role of carbon dots

Yaru Li, Zhongmin Liu, Yongchuan Wu, Jitao Chen, Jingyu Zhao, Fengmin Jin, Ping Na*

School of Chemical Engineering and Technology, Tianjin University, Tianjin 300354, China

ARTICLE INFO

Keywords:
Carbon dots
TiO_2 nanosheets
Photoreduction
Cr(VI)

ABSTRACT

Carbon dots-TiO_2 nanosheets (CDs-TNs) composites were synthesized by hydrothermal method and applied for the first time in photoreduction of Cr(VI) under sunlight illumination. The materials were characterized by transmission electron microscope, X-ray diffraction, thermogravimetric analysis, Fourier transform infrared spectrometer, and X-ray photoelectron spectroscopy analysis. The results confirmed that CDs are successfully incorporated with TNs through Ti—O—C bonds. With the introduction of CDs, CDs-TNs composites exhibit excellent photoreduction performance of Cr(VI), which is higher than that of TNs, P25 and CDs-P25. The unique upconversion property and electron transfer property of CDs play essential roles on light harvesting and charge carriers transferring in the photoreduction process. Most importantly, CDs could facilitate the formation of H_2O_2, leading to the consumption of holes. As a result, the recombination of photoinduced electron-hole pairs is hindered and photoreduction activity of CDs-TNs is promoted.

1. Introduction

Chromium (Cr), mainly consisting of hexavalent chromium (Cr(VI)) and trivalent chromium (Cr(III)), is one of toxic heavy metals in nature [1]. Compared with Cr(III), Cr(VI) with higher mobility is more toxic and carcinogenic, hence the treatment of Cr(VI) wastewater is the principal emphasis in Cr pollution control. It is well known that Cr(VI) is irreplaceable in industries such as metallurgical, refractory and chemical industries, which inevitably caused the release of Cr(VI) into natural water and drinking water [2]. Therefore, it is urgent for us to remove Cr(VI) from polluted wastewater. The favorable strategy is to reduce Cr(VI) to less harmful Cr(III) through the reduction process, and then precipitate Cr(III) in the form of $Cr(OH)_3$ at neutral or alkaline pH [3,4]. Among various reduction processes, photoreduction exhibits green approach, low treatment cost, and stable performance, which has been studied extensively and emerged as a promising method for Cr(VI) reduction [4,5]. In numerous photocatalytic materials, titanium dioxide (TiO_2) has been widely used to photoreduction due to its high activity, chemical stability and low cost [6]. However, pure TiO_2 still remain some limitations: (i) it could only response ultraviolet (UV) light because of the wide band gap [7]; (ii) its photoinduced electron-hole pairs are easy to recombine due to the kinetically slow holes consuming reaction [8]. These defects result in the lower solar energy utilization and photoreduction activity of TiO_2. Therefore it is essential to modify TiO_2 and overcome its weaknesses.

Generally, there are two common kinds of methods to modify TiO_2. One way is to change the phase structure, crystallinity, or morphology of TiO_2. For instance, since (001) facets are more reactive than other facets, anatase TiO_2 nanosheets (TNs) with high exposed (001) facets are proved to present better performance than P25 or regular TiO_2 both in photo oxidation and reduction [9,10]. The other approach is to combine TiO_2 with various ions, noble metals, semiconductors or other materials by doping, deposition, or sensitization [7,11–16]. In particular, carbon materials (active carbon, carbon nanotubes, carbon membrane, graphene, etc.) modified photocatalysts possess a better photocatalytic activity because that the combination with carbon materials could not only extend the photoresponse into visible range but also promote the separation of photoinduced electron-hole pairs [17–21]. However, even though the above carbon materials possess large specific surface area, their large size may cause the aggregation of TiO_2 particles.

Presently, a new carbon material—carbons dots (CDs)—has attracted considerable attention. CDs possess small size, high dispersion, abundant surface functional groups, unique photoluminescence and electron transfer property [22,23], which not only possess advantages of quantum dots and carbon materials [24,25], but also can avoid the coagulation problem of TiO_2 when combined with TiO_2. Therefore, CDs could be a better dopant in modifying TiO_2 without limiting their performance. In addition, Zeng [26] discovered that CDs could boost the generation of H_2O_2 in photocatalytic water disinfection process, and

* Corresponding author.
E-mail address: naping@tju.edu.cn (P. Na).

http://dx.doi.org/10.1016/j.apcatb.2017.10.023
Received 29 July 2017; Received in revised form 25 September 2017; Accepted 11 October 2017
Available online 12 October 2017
0926-3373/

Liu [27] found that system with higher H_2O_2 concentration showed higher photocatalytic reduction of Cr(VI) than that with lower H_2O_2 concentration. On these grounds, it is possible that CDs modified TiO_2 photocatalytic system could produce more H_2O_2 in the reaction and exhibit higher photoreduction activity.

In fact, some CDs-TiO_2 composites have been prepared and proved to have better performance in photodegradtion of organic dyes, photocatalytic hydrogen evolution and photoelectrochemical fields [28–30]. However, to our knowledge there is no report in the literature work on the photoreduction Cr(VI) by CDs-TiO_2 composites and the role of CDs in photoreduction of Cr(VI) system has not been detailedly researched. Hence, it is necessary to dive into the photoreduction capability and mechanism for Cr(VI) of CDs-TNs.

In this paper, carbon dots-TiO_2 nanosheets (CDs-TNs) composites were prepared by decorating carbon dots on TiO_2 nanosheets through hydrothermal reaction. The morphology, phase, chemical composition and optical properties of CDs-TNs were characterized. Then, CDs-TNs were applied to photocatalytic reduction of Cr(VI). CDs-TNs showed more excellent performance than that of pure TNs, P25 and CDs-P25. Finally, the possible role of CDs and photoreduction mechanism were proposed based on the experimental results.

2. Materials and methods

2.1. Materials

Tetrabutyl titanate (TBOT), citric acid monohydrate (CA), scopoletin ($C_{10}H_8O_4$, ≥98%), 1, 5-diphenylcarbohydrazide (DPC) and horseradish peroxidase (HRP, ≥300 units/mg) were obtained from Aladdin Reagent Company. Absolute ethanol, concentrated ammonia solution ($NH_3{\cdot}H_2O$, 28 wt%), hydrofluoric acid (HF), acetone, potassium dichromate ($K_2Cr_2O_7$), concentrated sulfuric acid (H_2SO_4), sodium hydroxide (NaOH), sodium tetraborate ($Na_2B_4O_7$) and sodium bromated ($NaBrO_3$) were purchased from Real & lead Chemical Reagent Co. Ltd (Tianjin, China). All the reagents were of analytical pure grade without further purification.

2.2. Synthesis of TiO_2 nanosheets (TNs)

The TNs were synthesized by a fluorine induced hydrothermal method [31]. 50 mL TBOT and 6 mL HF were added into 200 mL Teflon-lined stainless steel autoclave which was then placed in an oven at 180 °C for 24 h. After cooling down to room temperature, the white products were collected by centrifugation and washed with 0.1 M NaOH to remove the F^-. Subsequently, the above precipitations were washed with deionized water and centrifugated until the supernatant was neutral. Finally, the solid samples were dried in an oven at 60 °C for 12 h.

2.3. Synthesis of carbon dots-TiO_2 nanosheets (CDs-TNs)

First, 1.05 g CA (0.2 M) were dissolved in 25 mL deionized water with magnetic stirring and the pH value of solution was adjusted to 6 by adding $NH_3{\cdot}H_2O$. Next, 0.4 g TNs were dispersed into the above solution. After 30 min stirring and sonication, the mixture was transferred into a Teflon-lined stainless steel autoclave with 100 mL capacity and maintained at 160 °C for 4 h. Finally, the product precipitates were obtained through centrifugation, followed by washing with deionized water and drying at 60 °C for 12 h.

In the hydrothermal reaction, CA were used as carbon source and $NH_3{\cdot}H_2O$ were used as base. CA and $NH_3{\cdot}H_2O$ could react first to form the amide bond between each other, and this intermediate subsequently transform to CDs through dehydrolysis reaction [32]. Accordingly, more CA added in reaction could produce CDs-TNs composites with higher content of CDs. Catalysts synthesized with different amount of CA (0.05 M, 0.1 M, 0.2 M and 0.4 M) were denoted as 0.05CDs-TNs, 0.1CDs-TNs, 0.2CDs-TNs and 0.4CDs-TNs, respectively.

2.4. Synthesis of carbon dots (CDs)

The CDs were prepared by the same method as described above without adding TNs. After reaction, the obtained solution was filtered with a 0.22 um microporous membrane to remove large particles and dialyzed through a dialysis bag (3500 MW) for 2 days. The CDs powders could be obtained by drying the above solution directly.

2.5. Characterization

The morphology, size and crystal lattice of materials were observed by Transmission electron microscopy (TEM, JEM-2100F, Jeol) at 200 kV. The crystalline phases of samples were identified by X-ray diffraction (XRD, D8Focus, Bruker AXS) under Cu Kα radiation (45 kV, 30 mA) with a scanning range from 10° to 80° at the speed of 5°/min. Fourier transform infrared spectrometer (FTIR) were performed by FTIR-8400S (Shimadzu) scanning from 4000 to 400 cm^{-1}. X-ray photoelectron spectroscopy (XPS, PHI5000VersaProbe, Ulvac-Phi) were measured by using the Mg Ka X-ray source with a base vacuum operated at 300 W. The content of CDs was analyzed by thermogravimetric analysis (TGA, SF/1382, Mettler-Toledo) in air atmosphere with a heating rate of 10 °C/min up to 800 °C. Zeta potentials of materials at different pH were measured using a Nano-ZS Zetasizer (Malvern Instruments). UV–vis absorption spectra of CDs solution were recorded on UV–vis spectrophotometer (Lambda 35, PerkinElmer). Photoluminescence (PL) spectra of liquid samples were performed by F-2500 Spectrophotometer (Hitachi) by using 700 V photomultiplier and 5 nm slit. UV–vis diffuse reflectance spectra (DRS) of powder samples were recorded on UV-2550 (Shimadzu) by using $BaSO_4$ as a reference. Photoluminescence (PL) spectra of solid samples were measured by Fluorolog3 spectrofluorometer (Horiba Jobin Yvon) with excitation of 325 nm wavelength. The Electrochemical impedance spectroscopy (EIS) measurements were carried out on a PGSTAT302N electrochemical workstation (Autolab) in a three-electrode system with platinum-carbon electrode as working electrode.

2.6. Photocatalytic experiments

The sunlight photocatalytic activity tests were carried out by a self-made four-channel reactor equipped with a Xenon arc lamp (500 W, Beijing Lighting Research Institute, China) to simulate sunlight irradiation and the light intensity in the reactant center was around 25.6 mW/cm^2. The visible light photocatalytic experiments were conducted by a single-channel reactor (CEL-HXF300, Ceaulight, China) under a 300 W Xenon arc lamp with a UV filter ($\lambda < 420$ nm) and the light intensity in the reactant center was around 540 mW/cm^2. The distance between the light source and reaction solution was 10 cm. The temperature of the reaction was kept at ambient temperature (20 °C).

In a typical procedure, 50 mg of catalysts were dispersed into 50 mL of aqueous Cr(VI) solution (10 mg/L) which was prepared by using $K_2Cr_2O_7$ as the source of Cr(VI). Before photocatalysis, the suspensions were adjusted by 0.2 M H_2SO_4 to maintain the pH value at 3 and stirred in the dark for 30 min to establish the adsorption-desorption equilibrium. After that, the Xenon arc lamp was turned on and the photocatalytic reaction began. The aliquots were taken out periodically and centrifuged at 12000 rpm for 3 min to remove the solid powders. The concentrations of Cr(VI) in the supernatant were measured by diphenylcarbazide (DPC) method [33] with UV–vis spectrophotometer (PerkinElmer Lambda 35) and the concentrations of total Cr were determined by inductively coupled plasma optical emission spectrometry (ICP-OES, Optima 4300DV).

In order to determine the influence of pH on Cr removal over materials, experiments under different pH value were conducted by the same procedure mentioned above. The pH values were adjusted from 1

to 11 with H_2SO_4 or NaOH.

2.7. Detection of H_2O_2 in the reaction

The detection of H_2O_2 in the reaction was conducted through a fluorometric scopoletin-HRP method by previous report [34]. The fluorescence intensity of scopoletin could be quenched when scopoletin reacted with H_2O_2 in the catalysis of HRP. Therefore, a higher fluorescence intensity of scopoletin means a lower concentration of H_2O_2. Firstly, the detecting solution was prepared by mixing 0.5 mL H_2O, 0.5 mL scopoletin solution (15 uM) and 0.025 mL HRP solution (0.1 mg mL^{-1}) with 10 mL supernatant after photocatalytic reaction. Secondly, 9 mL of above detecting solution together with 0.3 mL of the saturated $Na_2B_4O_7$ solution were transferred to a colorimetric tube. After 1 min shaken, the fluorescence intensity was measured by fluorescence spectrophotometer with excitation of 390 nm light.

3. Results and discussion

3.1. Characterization of TNs, CDs and CDs-TNs

The TEM and particle size distributions images of materials are illustrated in Fig. 1. It can be observed from Fig. 1(a and b) that pure TNs exhibit rectangular sheet-like structure with 30–50 nm side length and 5 nm thickness, and the interplanar distances of 0.235 nm and 0.351 nm correspond to the anatase TiO_2 (001) and (101) planes, respectively. The image of CDs (Fig. 1c) shows that the single CDs display circular outline and disperse well. From Fig. 1d, we can see that pure CDs are uniform with the average size of 1.95 ± 0.25 nm. Fig. 1e shows the image of 0.2CDs-TNs, where CDs deposit on the surface of TNs dispersedly, indicating CDs and TNs are coupled together. The lattice spacing of CDs in inset figure is 0.205 nm, which could be assigned to the (102) planes of graphitic (sp^2) carbon [35]. The diameter of CDs in 0.2CDs-TNs is 1.87 ± 0.26 nm (Fig. 1f), which is approximate to the pure one, indicating that the combination with TNs does not affect the size of CDs.

Fig. 2 shows the XRD patterns of CDs, TNs and CDs-TNs with different CDs content. The curve of CDs exhibits a broad peak centered at 21.5°, which is attributed to (002) planes of graphitic carbon [36]. And the calculated interlayer spacing (0.405 nm) is larger than that of graphite (0.334 nm), probably resulting from the introduction of oxygen-containing functional groups at the edge of CDs [37]. In the curves of CDs-TNs and TNs, the peaks located at 25.28°, 37.80°, 48.05°, 53.89°, 55.06°, 62.69°, 68.76°, 70.31°, 75.03° are the characteristic diffraction peaks of anatase phase TiO_2 (PDF No. 21-1272). The peaks of CDs-TNs with different CDs content are identical to that of pure TNs without any shift, meaning that the addition of CDs would not change the phase of TNs. Besides, the typical broad peak at 21.5° can be found in CDs-TNs composites, and this peak becomes stronger with the increase of CDs content, confirming the existence of CDs onto TNs.

In order to determine the amount of CDs loaded on TNs, thermogravimetric analysis of TNs and CDs-TNs with different CDs content were conducted as shown in Fig. 3. Both of TNs and CDs-TNs composites have two stages of weight losses that can be observed in the TGA curves. Below 200 °C, the 3.9% weight loss is contributed to the evaporation of adsorbed water [29]. Between 200 °C and 700 °C, the 3.2% weight loss in TNs may results from the decomposition of surface-attached water, −OH groups and residual organic compound, while more weight loss observed in CDs-TNs composites can be ascribed to the combustion of CDs [29,38,39]. Therefore, the content of CDs in 0.05CDs-TNs, 0.1CDs-TNs, 0.2CDs-TNs and 0.4CDs-TNs account for ca. 1.67%, 1.88%, 2.00% and 2.16%, respectively. In hydrothermal reaction, as not all CA can transform to CDs and some organic substances are formed [40], which cannot be adsorbed onto TNs and remain in the solution, causing actual CDs-loading amount is not in proportion to the adding amount of CA.

The FTIR spectra (Fig. 4) of CDs, TNs and 0.2CDs-TNs were carried out to study the bonding composition and functional groups of materials. All spectra display absorption peaks at 3427, 1630 and 1384 cm^{-1}, which are assigned to O−H stretching vibration of adsorbed water, bending vibration of hydroxyl groups and skeletal vibration of symmetric carboxylate (C═O) stretching, respectively [38,41]. Besides, the vibration peaks of N−H (3220 cm^{-1}), COOH (1705 cm^{-1}), C−N = (1441 cm^{-1}) can also be observed in CDs [42], signifying the presence of carboxylic and amide groups on the surface of CDs. Compared with TNs, 0.2CDs-TNs possess some new features. The C═O peak becomes stronger and the peak of C−O−C at 1257 cm^{-1} [43] is appeared, indicating the successfully coupling of CDs with TNs. What's more, a new peak of C−O at 1060 cm^{-1} and a shift of the broad absorption band below 1000 cm^{-1} can be observed, suggesting the formation of Ti−O−C bonds in CDs-TNs composites [38,43,44].

In order to further delve the chemical composition of CDs-TNs, XPS of 0.2CDs-TNs was conducted as shown in Fig. 5. The full survey spectrum (Fig. 5a) depicts that the composites contain the elements carbon, oxygen, titanium and nitrogen. Fig. 5b presents the deconvoluted high resolution C1 s spectrum of 0.2CDs-TNs, where three peaks at 284.6, 286.3 and 288.4 eV can be attributed to C−C & C═C (graphite), C−O and C═O [45], manifesting the existence of CDs on the surface of 0.2CDs-TNs. The O1s spectrum (Fig. 5c) fitted into three peaks at 529.8, 531.6 and 533.0 eV are corresponding to Ti-O, C−O and O−H, indicating the formation of Ti−O−C bonds between CDs and TNs [46]. Moreover, the binding energies of $Ti2p_{3/2}$ and $Ti2p_{1/2}$ are located at 458.5 and 464.2 eV (Fig. 5d), which have slightly shifted in comparison to the pure TNs [9], further supporting the formation of Ti−O−C bonds in CDs-TNs composites.

Before photocatalytic study, it is essential to explore the photoresponse properties of materials, so the UV–vis absorption spectra, PL spectra and UV–vis diffuse reflectance spectra of samples were conducted in Fig. 6. As shown in Fig. 6a, CDs exhibit a broad absorption in the range 200–650 nm with a peak concerted at 335 nm, which is mainly ascribed to the $n \rightarrow \pi^*$ transition of C═O [47]. The PL spectra of CDs behave excitation-dependent. As the excitation wavelength changing from 300 to 500 nm, the emission peak shifts from 430 to 550 nm, while as the excitation wavelength increases from 550 to 650 nm, the emission peak shifts from 450 to 430 nm. Significantly, CDs display upconversion PL behavior with excitation wavelengths from 550 to 650 nm. CDs with this upconversion property are promising energy-transfer component, which could help the composites utilize solar energy more efficiently [28]. As for UV–vis diffuse reflectance spectra of samples (Fig. 6b), CDs-TNs and TNs exhibit nearly same absorption edge, implying that carbon are just loaded on the TNs in the form of CDs and not incorporated into the TNs lattice [48]. Pure TNs show almost no absorption in visible region, while the CDs-TNs composites reveal an increasing absorption with the increasing amount of CDs, corresponding to the color of materials changing from white to brown. This indicates that CDs play a key role in enlarging the light wavelength range from ultraviolet light to visible light.

3.2. Photoreduction activity of materials

The dark adsorption and photocatalytic activities of TNs and CDs-TNs with different CDs content were evaluated by photoreduction of Cr (VI) (10 mg/L) in an aqueous solution under simulated sunlight irradiation, as shown in Fig. 7a. Fig. 7b depicts the corresponding kinetic curves fitted with a pseudo-first-order kinetic equation:

$$-\ln (C/C_0) = k\ t \quad (1)$$

Where C/C_0 is the relative concentration of residual Cr(VI), k is the apparent reaction rate constant and t is the irradiation time, respectively. It can be observed that pure TNs could only photoreduce 34.9% Cr(VI) and all CDs-TNs composites could photoreduce 95% Cr(VI) after

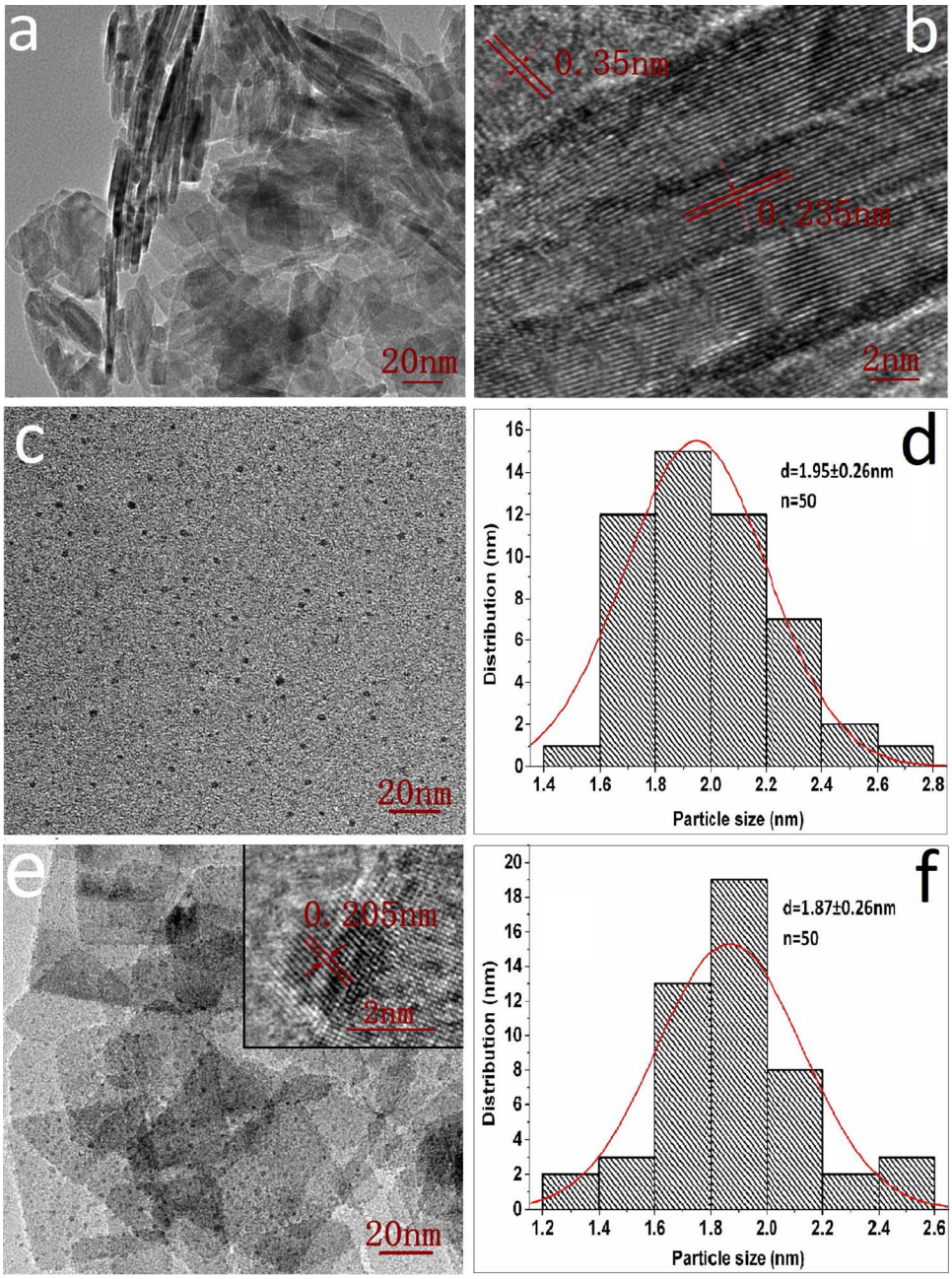

Fig. 1. (a) TEM image and (b) HR-TEM image of TNs; (c) TEM image of pure CDs; (d) Particle size distributions of pure CDs; (e) TEM and HR-TEM (inset) image of 0.2CDs-TNs; (f) Particle size distributions of loaded CDs.

photoreaction. With the amount of CDs increasing, the reaction rates and photoreduction activities of CDs-TNs composites increase firstly and then decrease. The application of 0.2 M citrate (CA) for generating CDs to modify TNs (0.2CDs-TNs) displays the highest photoreduction capability: the photoreduced Cr(VI) is over 99.2% after 120 min irradiation, and the corresponding reaction rate ($k = 0.027\ min^{-1}$) is 9 times than that of pure TNs ($k = 0.003\ min^{-1}$). When the CA content is lower than 0.2 M, the photoreduction efficiency of composites increases gradually with the increased CDs amount, indicating that the introduction of appropriate amount CDs have positive influence on improving photoreduction performance of composites. However, further increasing the amount of CA will bring about a significant decrease of photoreduction activity, probably owning to the reduced catalytic active sites and increased charge carriers recombination rate caused by excessive CDs loaded on materials [46,49]. Therefore, the optimal dosage of CA is 0.2 M in the hydrothermal reaction, and the corresponding product (0.2CDs-TNs) present the best photoreduction activity.

The pH value of Cr(VI) solution, which determines the species of Cr (VI) and surface charge of materials, has a great influence on the performance of photocatalysts. Accordingly, the effect of solution pH value on the adsorption and photoreduction of Cr(VI) by 0.2CDs-TNs and pure TNs is evaluated. Fig. 8a depicts Cr removal ability of 0.2CDs-TNs. In the process of adsorption, the optimum pH of 0.2CDs-TNs is 3. When pH value is 1, the majority of Cr(VI) are presented in the form of neutral H_2CrO_7, which has a lower affinity for CDs-TNs, leading to weaker adsorption ability for Cr(VI) than that at pH 3. When pH ≥ 3, the adsorption ability of samples decreases with the increase of pH because the surface of CDs-TNs could carry more positive charges at lower pH which is favorable to attract negatively-charged species $HCr_2O_7^-$ or CrO_4^{2-} (main forms of Cr(VI) at pH ≥ 2) through electrostatic forces [50].

For photoreduction of CDs-TNs, the reduction efficiency of Cr(VI) decreases with the increase of pH. CDs-TNs display over 99.9% removal efficiency of Cr(VI) at pH 1, whereas only 4.1% Cr(VI) could be reduced

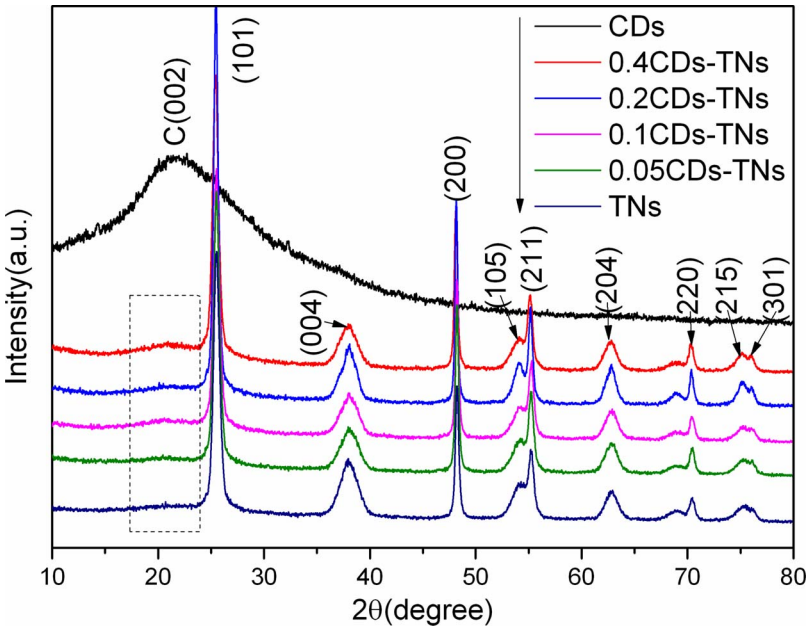

Fig. 2. XRD patterns of CDs, TNs and CDs-TNs with different CDs content.

at pH 11. The photoreduction of Cr(VI) basically proceeds the following reactions [27]:

pH 1: $H_2CrO_7 + 6H^+ + 3e^- \rightarrow Cr^{3+} + 4H_2O$ (2)

pH 2–6: $HCrO_7^- + 7H^+ + 3e^- \rightarrow Cr^{3+} + 4H_2O$ (3)

pH 7–14: $CrO_4^{2-} + 4H_2O + 3e^- \rightarrow Cr(OH)_3 + 5OH^-$ (4)

Based on Le Chatelier's principle, H^+ favors the reduction in acidic solution, whereas OH^- shows an adverse effect in alkaline medium. Thereby, the lower pH brings about the higher photoreduction efficiency of Cr(VI).

It is also observed from Fig. 8a that Cr(III) appeared in solution at pH < 5, resulting in more residual total Cr detected in solution. When pH value is lower than 3, CDs-TNs are positively charged, which have a weak interaction with Cr^{3+} (main forms of Cr(III)). As pH increased to 5, the surface of CDs-TNs become negatively charged and could adsorb more Cr^{3+}. As pH continued to increase, the dominant species of Cr(III) are $Cr(OH)_3$, which could precipitate in solution or deposit on the catalyst, resulting nearly no Cr(III) detected as pH ≥ 5 [27]. Despite Cr (III) is less harmful and more manageable than Cr(VI), excessive Cr(III) would be reoxidized to Cr(VI) [39] and increase the difficulty of removal work. Accordingly, we choose 3 as optimal removal pH value with comprehensive considering of removal efficiency of total Cr.

Cr removal efficiency by pure TNs with varying pH is conducted as shown in Fig. 8b. Pure TNs get the best adsorption on pH of 3 and the best photoreduction efficiency on pH of 1, which is consistent with CDs-TNs. Contrary to that of 0.2CDs-TNs (pH_{pzc} = 4.50, Fig. S1), pure TNs (pH_{pzc} = 6.05, Fig. S1) possess positively charged surface at pH 5, which has weak attraction to Cr^{3+}, leading to a small amount of Cr(III) still remained in solution after treated by TNs. Meanwhile, the photoreduction ability of pure TNs is weaker than that of CDs-TNs in varies pH, indicating the favorable effect of CDs in CDs-TNs composites.

Fig. 9 demonstrates a comparison of reduction performances of CDs, TNs, P25, 0.2CDs-TNs, 0.2CDs-P25 and 0.2CDs + TNs (the mechanical mixture of CDs and TNs) toward Cr(VI) solution at pH 3 under simulated sunlight irradiation. The adsorption process of Cr(VI) onto

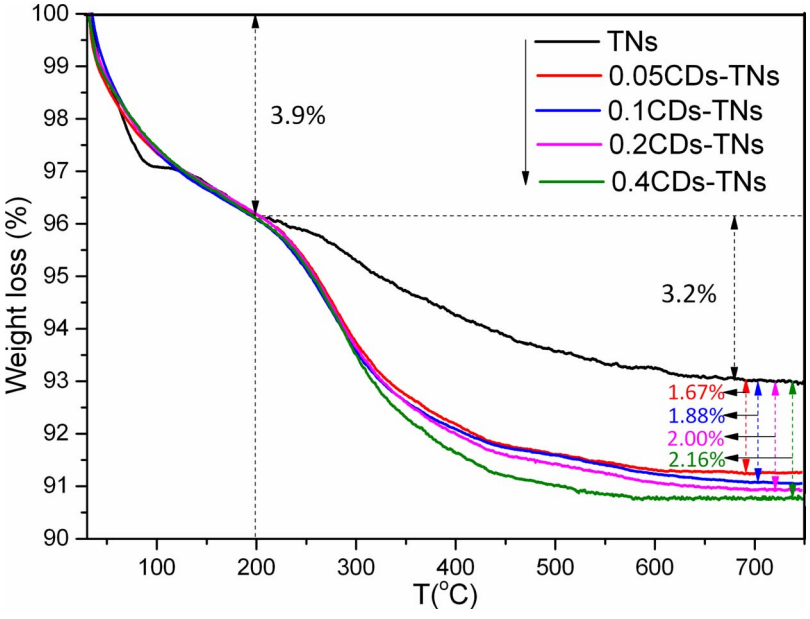

Fig. 3. TGA curves of TNs and CDs-TNs with different CDs content.

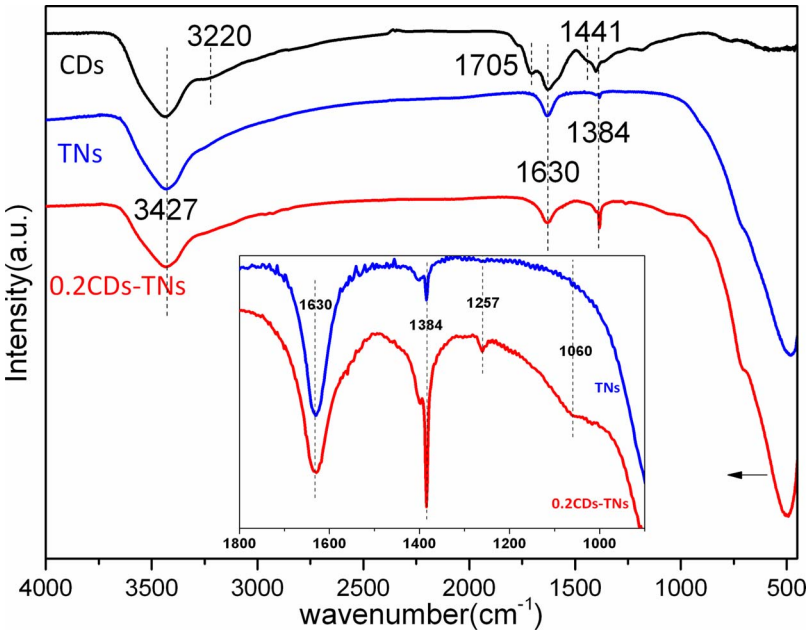

Fig. 4. FTIR spectra of CDs, TNs and 0.2CDs-TNs. The inset is a comparison between the FTIR spectra of TNs and 0.2CDs-TNs in the range of 900–1800 cm^{-1}.

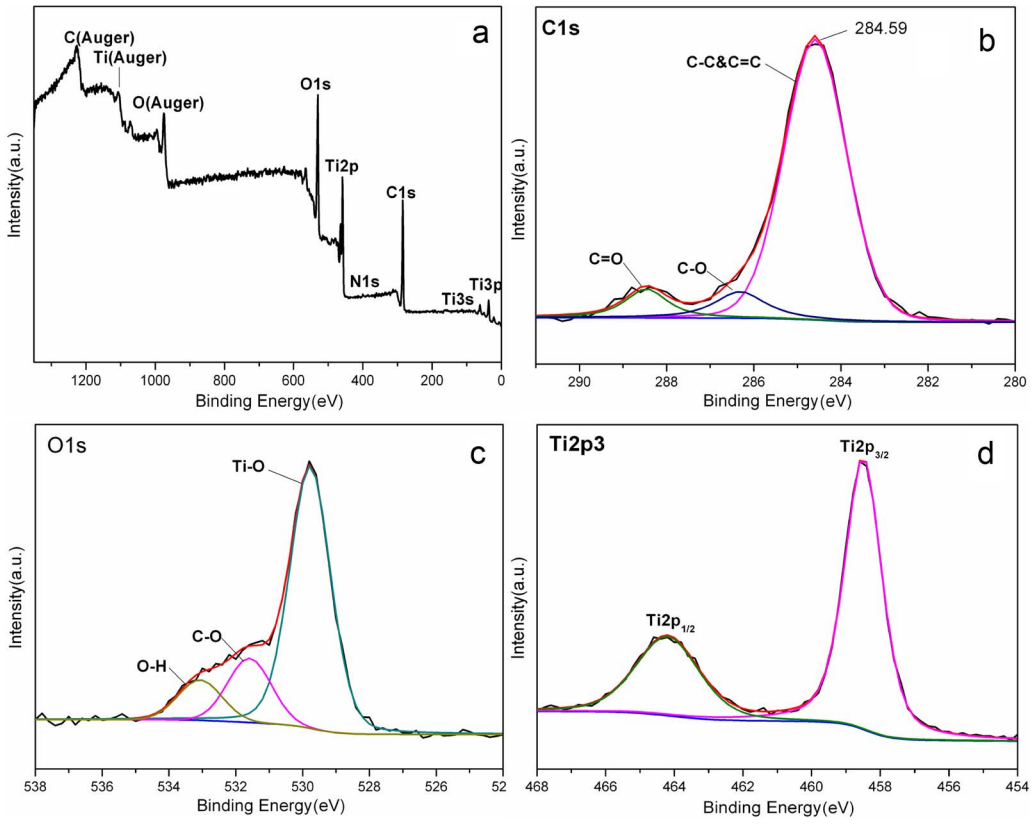

Fig. 5. (a)The full survey XPS spectrum, the deconvoluted XPS spectra of (b) C1s, (c) O1 s and (d) Ti2p of 0.2CDs-TNs.

materials is fast, which almost achieve equilibrium within 15 min. After 30 min, all materials can reach the adsorption-desorption equilibrium, which is consistent with the relative literatures [10,51]. The concentration of Cr(VI) has dropped by 3% for pure CDs in dark process, perhaps due to the redox reaction occurred between CDs and Cr(VI) [52]. After 120 min irradiation, the concentration of Cr(VI) remains nearly unchanged, suggesting that CDs have no photoreduction capability for Cr(VI). In terms of TiO_2 based materials, the adsorption capacity of Cr(VI) is in order of 0.2CDs-TNs > 0.2CDs + TNs > TNs > 0.2CDs-P25 > P25. As for photoreduction abilities of materials, P25 only photoreduce about 15.6% of Cr(VI) in 120 min, while TNs could reduce twice Cr(VI) than P25. The higher photoactivity of TNs is attributed to their large percentage of (001) facets which present higher surface energy and reactivity than (101) facets of P25 [53]. When modified by CDs, the photoreduction efficiency of Cr(VI) for P25 and TNs have increased to 67.8% and 99.2% within the same reaction time, showing that CDs have a positive effect on the photoreduction. In addition, even though 0.2CDs-TNs and mix 0.2CDs + TNs have the same CDs loading, the photoreduction activity of the former is 25% higher than that of the latter. This result confirms that the Ti—O—C

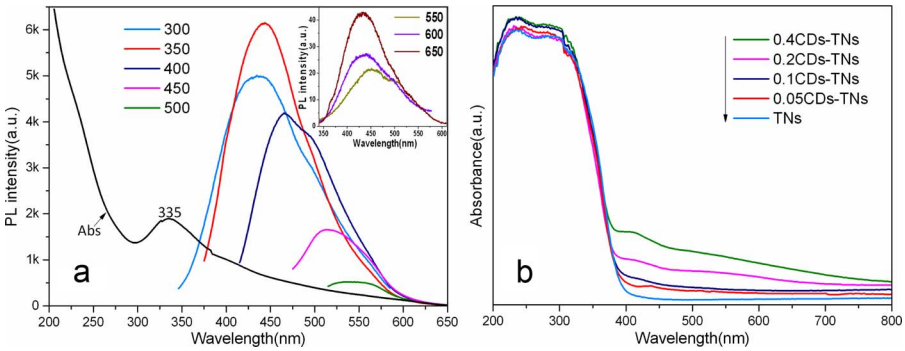

Fig. 6. (a) UV–vis absorption spectra (Abs) and PL spectra of CDs with excitation wavelengths from 300 to 500 nm, Inset: Upconverted PL spectra of CDs with excitation wavelengths from 550 to 650 nm; (b) UV–vis diffuse reflectance spectra of TNs and CDs-TNs with different CDs content.

bonds between TNs and CDs formed by hydrothermal treatment are more helpful to photoreduction performance than the simple electrostatic interactions.

Cr(VI) reduction performances of CDs, TNs, P25, 0.2CDs-TNs, 0.2CDs-P25 and 0.2CDs + TNs at pH 3 under visible light are also evaluated in Fig. S2. Under visible light, the photoreduction ability sequence of materials is as follows: 0.2CDs-TNs > 0.2CDs + TNs > 0.2CDs-P25 > TNs > P25 > CDs, which is the same as that under sunlight, suggesting that CDs-TNs also exhibit excellent performance under visible light illumination. Besides, the photoreduction rate of Cr(VI) by 0.2CDs-TNs under visible light is faster than that under sunlight, and the photoreduction efficiency can reach 99.9% within 90 min. This difference can be explained by the different light intensity and photocatalytic reactor. Although the power rating of 300 W Xenon arc lamp is lower than 500 W Xenon arc lamp, the actual light intensity in sunlight reactor is around 540 mW/cm^2, which is much higher than that in sunlight reactor. Besides, the visible light photocatalytic activity tests were carried out by a self-made single-channel reactor, which has lower efficiency than that four-channel reactor employed in sunlight photocatalytic activity tests. Therefore, these factors boost the photoreduction performance of materials in sunlight reactor.

The repeatability experiment of 0.2CDs-TNs is investigated as shown in Fig. S3. After photoreduction, the used 0.2CDs-TNs were soaked in 1 M $NaBrO_3$ solution to remove Cr(III) and washed with 1 M NaOH solution to regenerate. The samples were reused in six cycles for photoreduction of Cr(VI). After one-cycle of photoreduction, the regenerated 0.2CDs-TNs exhibit a gradually decreased performance during the next three cycles and then keep nearly stable in the fifth and sixth cycle. In the sixth cycle, even though Cr(VI) reduction ratio of 0.2CDs-TNs decreases to 40%, it still higher than that of unused TNs. The decreased performance could be explained that part of CDs may be washed off during the regenerated process, corresponding to the brown color of 0.2CDs-TNs becoming lighter after regenerated. This phenomenon further confirms the essential role CDs for improving the photoredcution performance of CDs-TNs composites.

3.3. Mechanism of photoreduction activity enhancement

The above photocatalytic activity results reveal that the performance of TNs improved significantly when conjuncted with CDs, manifesting that CDs play a favorable role in the enhancement of photocatalytic activity of composites.

On one hand, CDs can absorb visible light in the range of 550–650 nm and emit shorter wavelengths, which are easier to be absorbed by composites (Fig. 6a). This upconversion property could make CDs to be promising energy-transfer component, increasing the efficiency in utilizing the visible light of the composites. As a result, the CDs modified TNs can be excited by a broad range of the sunlight, and exhibit higher photoreduction efficiency under simulated sunlight.

On the other hand, CDs are reported to serve as electron reservoir and donor in photocatalytic process [26,46], and it is possible for CDs to trap electrons from the conduction band of semiconductor and donate them to reduction reaction. As a result, CDs could promote photogenerated carriers' separation and transportation, enhancing the photocatalytic activity of CDs-TNs. The PL and EIS tests shown in Fig. 10 verify the above functions. Fig. 10a displays the PL spectra of TNs and CDs-TNs with different CDs content under excitation of 325 nm. The higher PL intensity means the higher recombination of electrons and holes. Compared with pure TNs, all CDs-TNs composites show lower PL intensity, revealing that the added CDs could hinder the recombination of charge carriers. Among CDs-TNs composites, 0.2CDs-TNs exhibit the lowest PL intensity, suggesting the least charge recombination. From the EIS Nyquist plots (Fig. 10b) we can see that pure TNs display the biggest arc radius and 0.2CDs-TNs display the smallest arc radius among all the samples, suggesting the highest charge transfer resistance across pure TNs, which signifies that the interfacial charges transfer more rapidly when modified TNs with CDs. Both PL and EIS analyses illustrate that with CDs content increasing, the charge carriers recombination rate decrease firstly and then increase. In the case of 0.2CDs-TNs, the recombination rate of photoinduced electron-hole pairs is lowest, contributing to their highest photoreduction activity. Excessive CDs may serve as recombination centers for charge carriers [49], bringing about lower photoreduction activity of 0.4CDs-TNs,

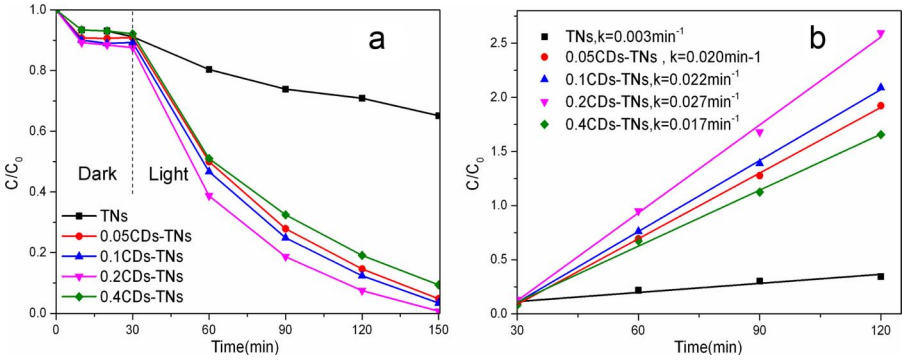

Fig. 7. (a) Photoreduction of Cr(VI) by CDs-TNs with different amount of CDs under simulated sunlight; (b) The corresponding fitted reaction kinetic curves ($-\ln(C/C_0) = kt$).

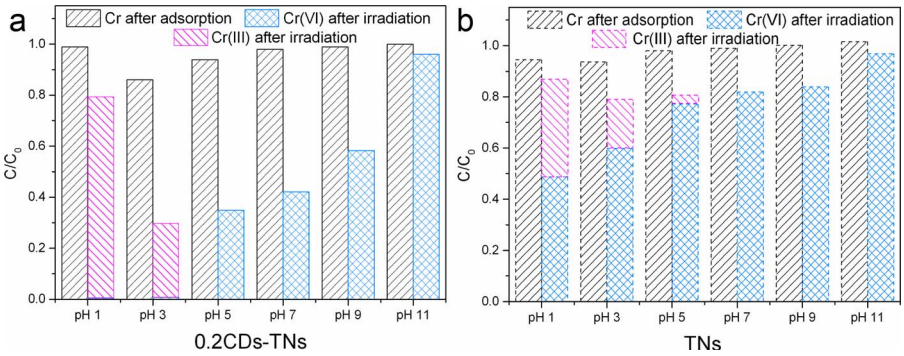

Fig. 8. Removal of Cr over (a) 0.2CDs-TNs and (b) TNs by 30 min adsorption and 120 min irradiation at pH = 1–11. C/C_0 is the relative concentration of residual Cr.

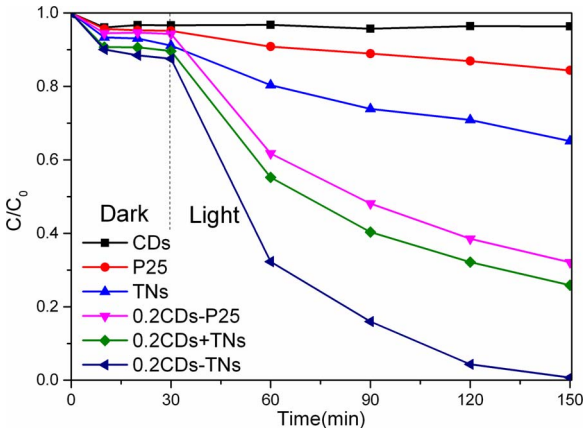

Fig. 9. Comparison of photoreduction of Cr(VI) of various samples under simulated sunlight.

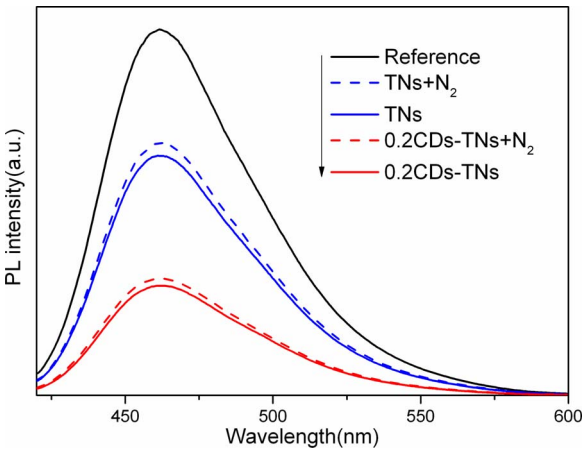

Fig. 11. Fluorescence intensity of scopoletin over TNs and 0.2CDs-TNs in Cr(VI) solution with or without N_2 bubbling after simulated solar irradiation. Reference is fluorescence intensity of scopoletin over pure water.

which consist with the above photocatalytic activity results.

In addition, at pH 3, the photoreduction of Cr(VI) on photocatalysts proceeded as follows [26,27,54]:

$$TNs + h\nu \rightarrow h^+ + e^- \quad (5)$$

$$HCrO_4^- + 7H^+ + 3e^- \rightarrow Cr^{3+} + 4H_2O \quad (3)$$

$$O_2 + 2H^+ + 2e^- \rightarrow H_2O_2 \quad (6)$$

$$h^+ + H_2O \leftrightarrow H^+ + \cdot OH \quad (7)$$

$$\cdot OH + \cdot OH \leftrightarrow H_2O_2 \quad (8)$$

TNs can be excited to generate conduction band electrons and valence band holes (Eq. (5)). Electrons can reduce Cr(VI) to Cr(III) (Eq. (3)) and react with dissolved oxygen to produce H_2O_2 (Eq. (6)), while holes can react with H_2O to form ·OH and then two ·OH combine with each other to form H_2O_2 (Eqs. (7), (8)). As H_2O_2 is an important product in the photoreduction process, which could evaluate the photoreduction activity of catalyst [27], it is necessary to detect H_2O_2 in TNs and CDs-TNs slurry systems. As shown in Fig. 11, the PL intensity of scopoletin in supernatant of samples after irradiation is lower than that in reference, implying that both TNs and 0.2CDs-TNs suspension could produce H_2O_2 under illumination. In both TNs and 0.2CDs-TNs systems, all the concentrations of H_2O_2 under N_2 atmosphere are slightly lower than that under air atmosphere, indicating that most of H_2O_2 is produced from H_2O oxidation and only a few H_2O_2 is coming from O_2 reduction. Comparing the amount of H_2O_2 generated in TNs and 0.2CDs-TNs systems, we can deduce that CDs could conduce to the formation of H_2O_2, which is consistent with the previous report [26]. Accordingly, for pure TNs system, because of the slow holes consumed rate by H_2O, electrons and holes would be easy to recombine, resulting in a poor photocatalytic performance of TNs. For 0.2CDs-TNs system, as CDs could facilitate the conversion of ·OH to H_2O_2 [26], the reaction equilibrium of Eqs. (7) and (8) can be shifted toward the right side, leading to the consumption of holes. As a result, CDs could suppress the recombination of electrons and holes and promote the photocatalysis

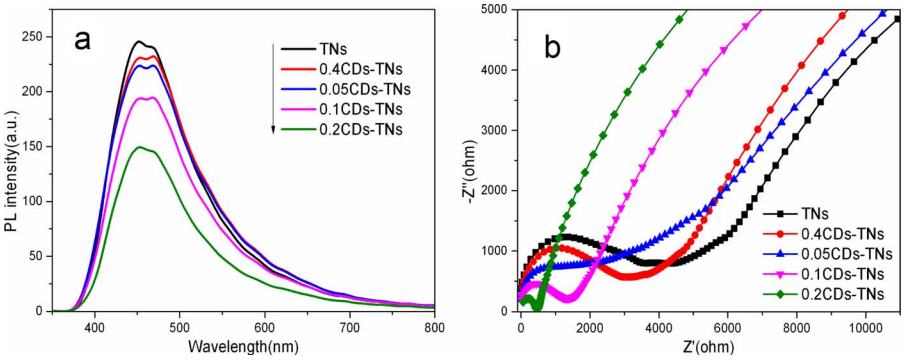

Fig. 10. (a) PL spectra and (b) EIS spectra of TNs and CDs-TNs with different CDs content.

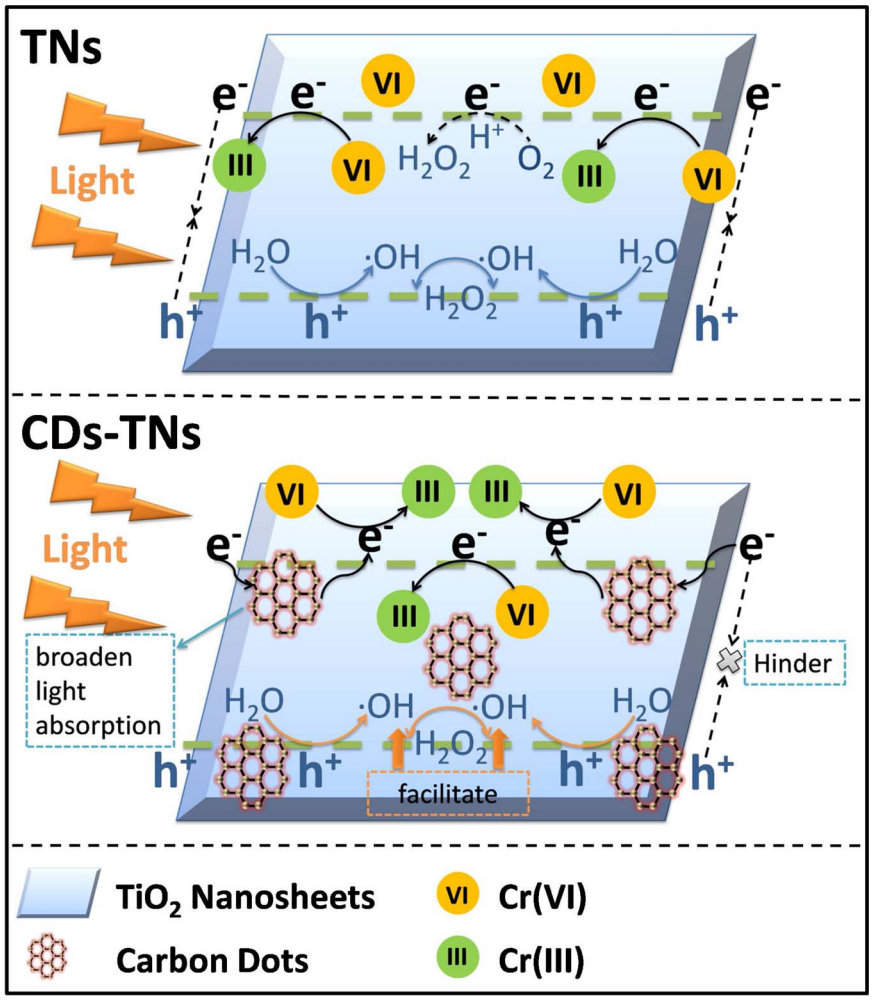

Scheme 1. Schematic illustration of Cr removal mechanism of TNs and CDs-TNs.

redox cycle unceasingly. In brief, CDs could enhance the photoreduction activity of composites by means of promoting the consumption of holes.

Scheme. 1 demonstrates the Cr(VI) photoreduction mechanism of TNs and CDs-TNs, as described above. The reason that CDs-TNs possess better performance in the removal of Cr(VI) than TNs can be attributed to the introduction of CDs, which broaden the light absorption range of composites, facilitate the separation and transportation of charge carriers, and promote the consumption of holes.

4. Conclusions

We have synthesized CDs-TNs composites through a hydrothermal approach and applied the composites to the photoreduction of Cr(VI). CDs are well uniformly dispersed on TNs by Ti—O—C bonds. 0.2 CDs-TNs exhibit the highest reaction rate ($k = 0.027\ min^{-1}$) and more than 99.2% Cr(VI) was reduced after 120 min irradiation. The CDs-TNs composites showed higher photocatalytic reduction efficiency for Cr (VI) than TNs, P25 and CDs-P25, which can be attributed to the highly active (001) facets and favorable effect of CDs. With the combination of CDs, the composites show efficient visible light absorption and enhanced charge transfer ability. What's more, CDs could facilitate the conversion of ·OH to H_2O_2, so as to accelerate the consumption of holes, and ultimately promote the photoreduction activity of CDs-TNs composites.

Acknowledgments

This work was supported by the National High Technology Research and Development Program of China (863 Program) (no. 2012AA063504), the National Natural Science Foundation of China (no. U1407116, 21511130020, 21276193), and the Tianjin Municipal Natural Science Foundation (no. 13JCZDJC35600).

Appendix A. Supplementary data

Supplementary data associated with this article can be found, in the online version, at http://dx.doi.org/10.1016/j.apcatb.2017.10.023.

References

[1] J.A. Alcedo, K.E. Wetterhahn, Int. Rev. Exp. Pathol. 31 (1990) 85–108.
[2] B. Annangi, S. Bonassi, R. Marcos, A. Hernández, Mutat. Res.–Rev. Mutat. 770 (2016) 140–161.
[3] C.E. Barrera-Díaz, V. Lugo-Lugo, B. Bilyeu, J. Hazard. Mater. 223–224 (2012) 1–12.
[4] Y. Li, Y. Bian, H. Qin, Y. Zhang, Z. Bian, Appl. Catal. B–Environ. 206 (2017) 293–299.
[5] H. Chen, Y. Shao, Z. Xu, H. Wan, Y. Wan, S. Zheng, D. Zhu, Appl. Catal. B–Environ. 105 (2011) 255–262.
[6] O. Ola, M.M. Maroto-Valer, J. Photochem. Photobiol. C 24 (2015) 16–42.
[7] Z. Lu, Z. Zhu, D. Wang, Z. Ma, W. Shi, Y. Yan, X. Zhao, H. Dong, L. Yang, Z. Hua, Catal. Sci. Technol. 6 (2016) 1367–1377.
[8] O. Carp, Prog. Solid State Chem. 32 (2004) 33–177.
[9] Q. Xiang, K. Lv, J. Yu, Appl. Catal. B–Environ. 96 (2010) 557–564.
[10] Z. He, Q. Cai, M. Wu, Y. Shi, H. Fang, L. Li, J. Chen, J. Chen, S. Song, Ind. Eng. Chem. Res. 52 (2013) 9556–9565.
[11] X. Cai, Y. Li, J. Guo, S. Liu, P. Na, Chem. Eng. J. 248 (2014) 9–17.
[12] S. Liu, N. Wang, Y. Zhang, Y. Li, Z. Han, P. Na, J. Hazard. Mater. 284 (2015)

171–181.
[13] G. Žerjav, M.S. Arshad, P. Djinović, J. Zavašnik, A. Pintar, Appl. Catal. B–Environ. 209 (2017) 273–284.
[14] Z. Lu, P. Huo, Y. Luo, X. Liu, D. Wu, X. Gao, C. Li, Y. Yan, J. Mol. Catal. A-Chem. 378 (2013) 91–98.
[15] Z. Lu, F. Chen, M. He, M. Song, Z. Ma, W. Shi, Y. Yan, J. Lan, F. Li, P. Xiao, Chem. Eng. J. 249 (2014) 15–26.
[16] C.Y. Lee, J.T. Hupp, Langmuir 26 (2009) 3760–3765.
[17] M. Li, B. Lu, Q. Ke, Y. Guo, Y. Guo, J. Hazard. Mater. 333 (2017) 88–98.
[18] K. Woan, G. Pyrgiotakis, W. Sigmund, Adv. Mater. 21 (2009) 2233–2239.
[19] Z. Lu, X. Zhao, Z. Zhu, Y. Yan, W. Shi, H. Dong, Z. Ma, N. Gao, Y. Wang, H. Huang, Chem.–Eur. J. 21 (2015) 18528–18533.
[20] Q. Huang, S. Tian, D. Zeng, X. Wang, W. Song, Y. Li, W. Xiao, C. Xie, ACS Catal. 3 (2013) 1477–1485.
[21] Y. Li, W. Cui, L. Liu, R. Zong, W. Yao, Y. Liang, Y. Zhu, Appl. Catal. B–Environ. 199 (2016) 412–423.
[22] L. Li, G. Wu, G. Yang, J. Peng, J. Zhao, J.J. Zhu, Nanoscale 5 (2013) 4015–4039.
[23] S.Y. Lim, W. Shen, Z. Gao, Chem. Soc. Rev. 44 (2014) 362–381.
[24] Y. Liang, S. Lin, L. Liu, J. Hu, W. Cui, Appl. Catal. B–Environ. 164 (2015) 192–203.
[25] W. Cui, W. An, L. Liu, J. Hu, Y. Liang, J. Hazard. Mater. 280 (2014) 417–427.
[26] X. Zeng, Z. Wang, N. Meng, D.T. McCarthy, A. Deletic, J. Pan, X. Zhang, Appl. Catal. B–Environ. 202 (2017) 33–41.
[27] W. Liu, J. Ni, X. Yin, Water Res. 53 (2014) 12–25.
[28] H. Li, X. He, Z. Kang, H. Huang, Y. Liu, J. Liu, S. Lian, C.H.A. Tsang, X. Yang, S. Lee, Angew. Chem. Int. Edit. 49 (2010) 4430–4434.
[29] J. Wang, M. Gao, G.W. Ho, J. Mater. Chem. A 2 (2014) 5703–5709.
[30] J. Bian, C. Huang, L. Wang, T. Hung, W.A. Daoud, R. Zhang, ACS Appl. Mater. Interface 6 (2014) 4883–4890.
[31] X. Han, Q. Kuang, M. Jin, Z. Xie, L. Zheng, J. Am. Chem. Soc. 131 (2009) 3152–3153.
[32] D. Qu, M. Zheng, L. Zhang, H. Zhao, Z. Xie, X. Jing, R.E. Haddad, H. Fan, Z. Sun, Sci. Rep.–UK 4 (2014) 5294.
[33] Z.A. Zakaria, Z. Zakaria, S. Surif, W.A. Ahmad, J. Hazard. Mater. 146 (2007) 30–38.
[34] L. Zhang, G.T.F. Wong, Talanta 48 (1999) 1031–1038.
[35] H. Wang, J. Zhuang, D. Velado, Z. Wei, H. Matsui, S. Zhou, ACS Appl. Mater. Interface 7 (2015) 27703–27712.
[36] H. Sun, N. Gao, K. Dong, J. Ren, X. Qu, ACS Nano 8 (2014) 6202–6210.
[37] L. Tang, R. Ji, X. Cao, J. Lin, H. Jiang, X. Li, K.S. Teng, C.M. Luk, S. Zeng, J. Hao, S.P. Lau, ACS Nano 6 (2012) 5102–5110.
[38] N.C.T. Martins, J. Ângelo, A.V. Girão, T. Trindade, L. Andrade, A. Mendes, Appl. Catal. B–Environ. 193 (2016) 67–74.
[39] Z. Chen, Y. Li, M. Guo, F. Xu, P. Wang, Y. Du, P. Na, J. Hazard. Mater. 310 (2016) 188–198.
[40] S. Zhu, X. Zhao, Y. Song, S. Lu, B. Yang, Nano Today 11 (2016) 128–132.
[41] J. Yu, Y. Su, B. Cheng, M. Zhou, J. Mol. Catal. A–Chem. 258 (2006) 104–112.
[42] S. Wang, Z. Zhu, Y. Chang, H. Wang, N. Yuan, G. Li, D. Yu, Y. Jiang, Nanotechnology 27 (2016) 295202.
[43] W. Wang, D. Wang, W. Qu, L. Lu, A. Xu, J. Phys. Chem. C 116 (2012) 19893–19901.
[44] S.X. Liu, X.Y. Chen, X. Chen, J. Hazard. Mater. 143 (2007) 257–263.
[45] Y. Cong, X. Li, Y. Qin, Z. Dong, G. Yuan, Z. Cui, X. Lai, Appl. Catal. B–Environ. 107 (2011) 128–134.
[46] H. Yu, Y. Zhao, C. Zhou, L. Shang, Y. Peng, Y. Cao, L. Wu, C. Tung, T. Zhang, J. Mater. Chem. A 2 (2014) 3344–3351.
[47] L. Lin, M. Rong, F. Luo, D. Chen, Y. Wang, X. Chen, Trac–Trend Anal. Chem. 54 (2014) 83–102.
[48] Q. Xiang, J. Yu, M. Jaroniec, Nanoscale 3 (2011) 3670–3678.
[49] Z. Ren, X. Liu, H. Chu, H. Yu, Y. Xu, W. Zheng, W. Lei, P. Chen, J. Li, C. Li, J. Colloid Interface Sci. 488 (2017) 190–195.
[50] Y. Ku, I. Jung, Water Res. 35 (2001) 135–142.
[51] B. Sun, E.P. Reddy, P.G. Smirniotis, Environ. Sci. Technol. 39 (2005) 6251–6259.
[52] J. Shen, S. Shang, X. Chen, D. Wang, Y. Cai, Sens. Actuators B–Chem. 248 (2017) 92–100.
[53] D. Zhang, G. Li, X. Yang, J.C. Yu, Chem. Commun. 29 (2009) 4381–4383.
[54] L.B. Khalil, W.E. Mourad, M.W. Rophael, Appl. Catal. B–Environ. 17 (1998) 267–273.